Role of Particle Geometry and Surface Contacts in Solid-Phase Reactions

J. Kostogorova and H. J. Viljoen
Dept. of Chemical Engineering, University of Nebraska, Lincoln, NE 68588

A. Shteinberg
ALOFT Corp., Berkeley, CA 94708

Given the surface areas of three different species A,B, and C, what is the most likely contact area between A and B? This problem finds many applications, but it is of specific importance in solid-phase reactions. Reactions in powder mixtures depend strongly on contact area between reactants, even when one species may melt. The surface of particles is meshed with small "tiles," and a combinatorial problem is formulated to map all tiles onto each other. The number of different contacts of n constituents is $\sum_{i=1}^{n} i$*; if pores are present, they are considered a constituent. The combinatorial problem for* $n > 3$ *is computationally overwhelming, but for two or three species, the desirable contacts can be calculated. The model was developed for contact between three different species (two species are included as a special case). This could constitute three different powders at 100% MTD, or a mixture of two powders that includes pores where the latter phase acts as a third species. The combinatorial approach is used to find the discrete probability-distribution function (PDF), viz., p(z, A, B, C), where z is the number of desirable contacts (for example, A|B), given the surface areas (A, B, C). The first moment of the PDF gives the expectancy value* Ψ *(A|B, A, B, C) for contact between species A and B . The theory was demonstrated by two examples. A simple contact problem is solved for two powders that also contain pores. The second example compares kinetic rates for different shapes and sizes of particles.*

Introduction

Surface contacts between powders play important roles in the physical properties of mixtures, sintering rates, and rates of chemical reactions. Surface contact between the constituents of a composite material determines its properties. A number of studies have been dedicated to the fundamental understanding and quantitative description of transport properties of composites. An important element of such an analysis is the surface-contact area between different species. For example, the thermal conductivity of a composite is affected by the Kapitza interfacial thermal resistance between constituent phases [cf. Nan et al. (2000) and references therein]. Another important application of an effective surface-contact theory is chemical reactions in powder mixtures.

Correspondence concerning this article should be addressed to H. J. Viljoen.

Rate expressions formulated for gas or liquid reactions are invariably of the form $f(T, P) \cdot g([C_A], [C_B], \ldots)$, like the familiar expression $r = k_0 e^{-E/RT} \cdot g([C_A],[C_B],\ldots)$. However, it is quite obvious that usage of concentrations is not acceptable in the case of solid–solid reactions. Instead, surface areas are relevant variables. Although descriptions for gas–solid reactions have recognized the importance of changing surface area, going all the way back to the shrinking-core model (Smith, 1981), solid–solid reaction models have not included particle contacts, geometry, and evolution of size to a reasonable level of sophistication. Highly structured cell models have been proposed for applications in combustion synthesis (Hwang et al., (1997). The cells have varying transport properties to reflect the randomness of the original packing. Varma et al. (2001) used a regular two-dimensional (2-D)

matrix of circular cylinders (with nominally flat sides) in contact. A number of cylinders are removed at random to model the porosity. This structured approach permits a simple description of transport properties and contact areas. However, powder compacts are packed randomly. The structured packing is only one possible outcome out of nearly infinite possibilities. Nature prefers to manifest itself in terms of the most likely outcome, as we daily experience with the Boltzmann distribution. Therefore, the structured packing will only be acceptable if the contact areas and transport properties that result from this arrangement coincide with, or lie close to, the expectancy values (that is, the most likely outcome).

Tamhankar and Doraiswamy (1979) reviewed different solid-phase reacting models. Based on the rate-limiting process, models have been proposed to account for product-layer diffusion, nucleation growth, and kinetically controlled reactions. Particle geometries of spheres, disks, and cubes have been considered. In most of these models the conversion is expressed as a function of time, and in some models additional variables are included to account for the change in volume due to reaction. Frade and Cable (1992) revisited the Jander, Ginstling, and Brouhstein and Valensi-Carter models and showed deviations from the models when solubility of the transporting species increases. Historically, these models have evolved primarily from gas–solid processes like combustion of solid fuel and slow oxidation processes like corrosion. Another interesting application of effective surface contact is found in geology. Porous sandstone consists of a fine network of pores that is filled with water. The rate of deposition of silica from the aqueous phase onto existing quartz surfaces depends on the liquid-surface contact area. But this area changes with time as the pore sizes are reduced (Kieffer et al., 1999).

During the past three decades, there has been an increasing interest in combustion synthesis. This process includes solid–solid reactions (that is, all reactants are initially solid), and it has been explored as an alternative route to manufacture carbides, nitrides, intermetallics, and oxides (Merzhanov, 1994). Merzhanov presented several mechanisms that further underscore the complexities of some of these mechanisms. For example, pure Mo and B do not react, but powders with small amounts of oxides react readily. Volatile suboxides form and act as carriers of reactants to reaction sites on other solids. Solid–solid reactions often precede solid–liquid reactions in the same system, even for constituents with high melting points, because eutectics form. Interesting developments have been observed for combustion synthesis of intermetallics. Anselmi-Tamburini and Munir (1989) conducted one of the first studies that addressed surface contacts in a quantitative manner. They studied a multilayered sample consisting of Ni and Al foils. The reaction was initiated at one end and they measured propagation velocities between 10 and 12 cm/s. These velocities are considerably higher than the propagation velocities in most powder systems. The thickness of the metallic layers is also important, as the results of Ma et al. (1990) indicate. They also studied the reaction of multilayered samples of Ni and Al. The thickness varied between 10 and 20 nm, and velocities of 4 ms^{-1} were measured.

Dyer et al. (1994), Dyer and Munir (1995), and Weihs (1997) measured velocities of 60–200 cm/s for multilayered samples prepared by electron-beam evaporation and sputtering. These studies are important because they mark the first attempts to quantify the effects of surface contact areas and geometry of the reactants. Thickness of the foils and contact area are related issues. Simplistically the contact area defines the base on which any product layer will form. The final thickness of this layer determines the diffusion length, and, hence, the time to reach completion of the reaction. Large contact areas and thin layers favor thin product films, while small contact areas and thick foils favor thicker product films. Of course, these are broad generalities and in certain cases processes, unique to a specific mechanism, could overshadow them. An example of such a process was given by Yudson et al. (1998), who developed an interesting model of solid–solid reactions that include the formation of interface roughness using stochastic differential equations to capture thermal fluctuations on the mesoscopic level (that is, particle size).

It is considerably more difficult to quantify surface-area contacts and mean geometry of powder and particulate systems than the ordered layers of foils. Tomasi and Munir (1999) reported on the effect of particle size for the Al_2O_3–ZrO_2–Nb system. Three different particle sizes of the reactants were studied, and not only did they find an increase in reaction rates with decreasing particle sizes, but a change from spin-mode to stable propagation of the reaction front.

In powder systems, it remains a popular practice to assign spherical geometry to particles, reducing the dimensional description to diameter. This assumption may be convenient, but not necessarily the best. When only one variable (that is, diameter) is used to describe the geometrical state of the particle, it is not possible to distinguish between spheres, needles, and platelets. However, the shape of particles strongly depends on the history of its manufacture. Powders produced by milling are often platelets, crystallization produces powders that could be shaped like polyhedra, with multifaceted surfaces, and powders produced from condensation of vapors are often spherical. The simplest way to account for shape effects is to assign the particle a rhombic geometry.

The focus of this contribution is on the use of combinatorics to determine the expectancy value for surface contacts. The method is illustrated by two examples: a simple contact problem and a comparative kinetics study to demonstrate the effects of particle size and shape. But first we introduce the mathematical model for surface contacts.

Mathematical Model

Basic approach

The concepts of the mathematical model are illustrated in Figure 1. Consider a collection of particles of three different species. Realistically, the particles may vary in shape and size, but in modeling studies it is common practice to assign spherical shapes to particles and describe variation by particle-size distribution alone. Since we want to recognize different shapes, but compromise complexity and expediency, we represent each species by an "average" particle shape, which may still be very complex. The next step is to assign a simpler geometric form to it, as illustrated in Figure 1a. The rectangular rhombus is our geometric shape of choice, since it goes beyond a spherical description to distinguish between quasi-

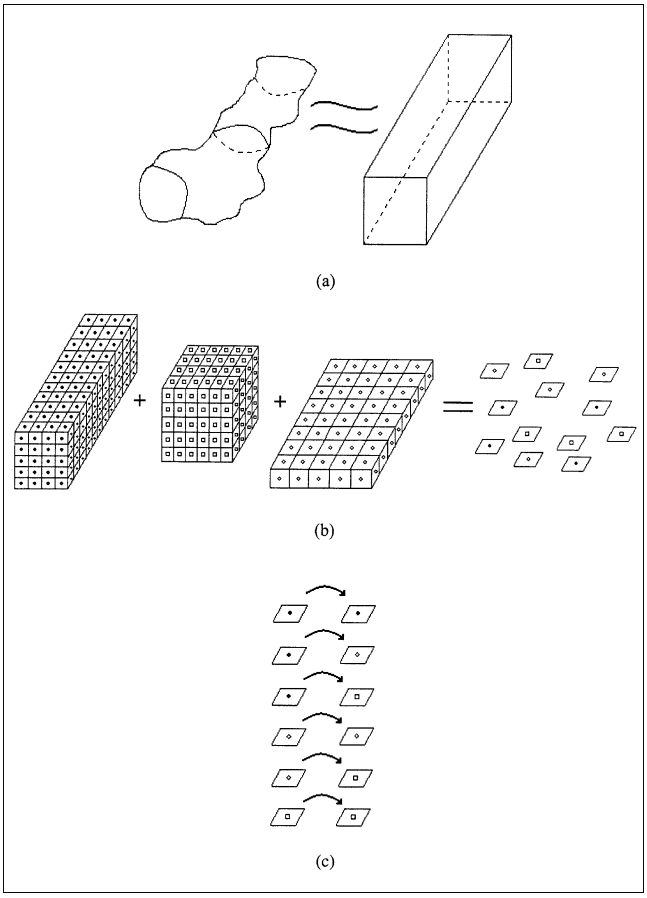

Figure 1. Geometric approximations of particles and mapping of surfaces.

spheres (cubes), platelets, and needles. Of course, geometric shapes, different from a rhombus, are also in order.

Remark. Surfaces scale in a fractal manner, but we restrict the description to rhombi with flat faces. It is also known that surface roughness, λ, measures the ratio of real surface area to geometrical surface associated with particle dimensions. As long as λ is known, it can be included in the current theory with no additional complexity, but we will use $\lambda = 1$.

Once typical shapes have been assigned to the three species, their particle-size distributions pertain to variations in the principal dimensions of the rhombi. Progressing from spheres to cylinders to rhombi, the principal dimensions vary from one to two to three, and the same number of size distributions is needed to characterize them. The first moments give the average lengths of the rhombi, and from here on we only consider averaged particles. The surfaces of the averaged particles are meshed with little square tiles. For that purpose we need a length scale and we opted to use a scaled Bohr radius. (Scaled radius is the side of a cube that contains an atom, instead of a sphere.) Of course, we use the same length scale for different species, because we want to map surfaces and not atoms.

In Figure 1b the meshing of the averaged particles of species A, B and C is shown. Note that the tiles are marked to distinguish between species (such as, $\bullet = A$, $\square = B$, and $\diamond = C$). The next step is to determine how many tiles of each species there are. Let d_L denote the length scale that defines a tile. The three principal dimensions of the A rhombus are expressed in terms of multiples of d_A as follows

$$(X_A, Y_A, Z_A) = d_L(K_A, L_A, M_A) \tag{1}$$

The number of tiles in one averaged particle of species A is N_{TA}

$$N_{TA} = 2\left[K_A L_A + K_A M_A + M_A L_A - 2(K_A + L_A + M_A) + 4\right] \tag{2}$$

Let N_A denote the number of particles of species A and the total number of tiles is

$$\sigma_A = N_A N_{TA} = 2N_A\left[K_A L_A + K_A M_A + L_A M_A - 2(K_A + L_A + M_A) + 4\right] \tag{3}$$

Note. We do not count edge tiles double, because tiles could be assigned to surface atoms and the latter should not be counted twice; however, for large values, the correction is very small.

The number of tiles in averaged particles of species B and C are calculated in the same way. The total number of tiles is

$$\Gamma = N_A N_{TA} + N_B N_{TB} + N_C N_{TC} \tag{4}$$

This is shown in the righthand side of Figure 1b. All these tiles are now bijectively mapped onto each other, but the identity mapping is excluded. This is shown in Figure 1c. In classic probability it is necessary that $(\sigma_A, \sigma_B, \sigma_C)$ are integers. A trivial scaling transforms σ_i back into the surface area

$$s_i = d_L^2 \sigma \tag{5}$$

Thus, all points on the surface of any given particle are in contact (associated/paired) with a unique point other than itself. It is further assumed that the powders are "ideally mixed." This means that any point x on any surface has no greater inherent affinity (probability) to be in contact with any other point y rather than a third point z (where $x \neq y \neq z$). One can physically interpret this ideal limit as the limit where *the effects of particle shape and size* in preferring a particular pattern of contacts *are minimized.* The larger the number of particles will be, the more correct this approach will be. The *independence* of mapping points implies that the outcome of one mapping does not influence the outcome of other points, even neighboring ones. This concept is both subtle and important. At first thought, the idea of points on the same face of a particle to be mapped onto different surfaces seems unrealistic, but the correctness of the approach lies exactly in the large number of particles. Whether it is required that all points on the same face of a rhombus must be mapped identically or independently, if a sufficiently large number of faces are considered, the outcome for either one of the approaches will be the same. The ergodicity of face–face pairing will overshadow the limitation of similar pairings of points on the same face.

Probability of A/B contact

Given three different species, A, B and C, we want to calculate the probability for contact between species A and B. The following definitions are introduced to convenience future calculations.

Definition 1. $\alpha = \min(\sigma_A, \sigma_B)$.

Definition 2. $\beta = \max(\sigma_A, \sigma_B)$.

In other words, if $\alpha = \sigma_A$ if $\sigma_A \le \sigma_B$, otherwise $\alpha = \sigma_B$.

$\Gamma = \alpha + \beta + \sigma_C$ is the sum of all the tiles that must be mapped. Using classic probability and the assumption of ideal mixing as defined, the fraction of the total area-on-area ($\Gamma/2$) that is A on B must be computed. We would like our solution to be unique, and it is accomplished by shrinking the squares into points. For that purpose we also introduce the following definitions.

Definition 3. $a = \alpha/\Gamma$.

Definition 4. $b = \beta/\Gamma$.

Definition 5. $c = \sigma_C/\Gamma$.

It is possible to express as α as $a \cdot \Gamma$ and mathematically execute the "shrinking" by letting $\Gamma \to \infty$. In the final analysis, we find that what really matters is the (dimensionless) fractions a, b, and c with the limit $\Gamma \to \infty$ being wholly independent of units, as the reader can verify. [Those familiar with a more modern probability theory might observe that the problem can be formulated in the language of functional analysis, but solving it would require "a measure over the operator-space of all bijective mappings of Γ onto itself." If this does not sound bad enough already, consider that this operator space we envision is likely to be unbounded and nonlinear, and all this would only make sense after adopting some topological labeling over the (expanding) domain making it into a vector space. (A vector space with no necessary physical meaning.).] As mentioned earlier, the correctness of the mapping lies in considering many tiles, and ideally $\Gamma \to \infty$. Also note that a and b are independent of the length scale d_L, and they can also be calculated in terms of surface areas, for example

$$a = \frac{\min(s_A, s_B)}{s_A + s_B + s_C}, \qquad b = \frac{\max(s_A, s_B)}{s_A + s_B + s_C} \qquad (6a,b)$$

The number of distinct ways that Γ can be paired is

$$N_{\text{pairs}} = \frac{\Gamma!}{(0.5\Gamma)!} 0.5^{\Gamma} \qquad (7)$$

($\Gamma!$ presents all permutations, divided by $[0.5\Gamma]!$, since the "order of the pairs" does not matter and the final term reflecting the fact that for our purposes the order within a pair does not constitute a unique event.) Also note that Γ must be even, a condition that becomes irrelevant when Γ becomes large. This is an expression for the total of all possible distinct events.

Let $Z \ge 0$ be the number of $A-B$ pairs. The same principles are used as before to calculate a Z number of $A-B$ pairs. It is obvious that the probability will be zero unless $0 < Z \le \alpha$.

Case 1: Two Species. When only species A and B are present, the probability for Z number of $A-B$ contacts is

$$P(Z, \alpha, \beta) = \frac{1}{Z!} \cdot \frac{\alpha!}{\left[\frac{\alpha - Z}{2}\right]!} \cdot \frac{\beta!}{\left[\frac{\beta - Z}{2}\right]!} \frac{\left[\frac{\Gamma}{2}\right]!}{\Gamma!} \cdot 2^Z \qquad (8)$$

Case 2: Three Species. When three species A, B, and C are present, $\sigma_C > 0$ and $\alpha + \beta < \Gamma$. The probability for Z $A-B$ pairs is now

$$P(Z, \alpha, \beta, \sigma_C) = \frac{\alpha!}{Z!} \cdot \frac{\beta!}{[\beta - Z]!} \cdot \frac{\left(\frac{\Gamma}{2}\right)!}{\Gamma!} \cdot 2^Z \cdot \sum_{k=0}^{\Delta} \frac{1}{k'!} \cdot \frac{1}{\left(\frac{\alpha - Z - k'}{2}\right)!} \frac{\sigma_C!}{[\sigma_C - k']!} \cdot \frac{((\beta + \sigma_C) - (Z + k'))!}{\left(\frac{(\beta + \sigma_C) - (Z + k')}{2}\right)!} \cdot 2^{k'} \qquad (9)$$

When Z is even, we define $\Delta = [\min(\alpha - Z, \sigma_C)]/2$ and $k' = 2k$. Alternatively, when Z is odd (consider 0 as even), $\Delta = [\min(\alpha - Z - 1, \sigma_C - 2)]/2$ and $k' = 2k + 1$. These formulas yield probability distribution curves for given α, β, and σ_C.

Note. Instead of α, β, and σ_C, we could also use a, b, and c: $P(Z, \alpha, \beta, \sigma_C) \equiv P(Z, a, b)$.

To illustrate Eq. 9, consider the problem of a 100 tiles, consisting of 20 tiles of type A, 30 of type B, and the balance of type C; thus, $\Gamma = 100$, $\alpha = \min(20,30)$, $\beta = \max(20,30)$. In Figure 2, the curve $D = P(Z, \alpha = 20, \beta = 30, \sigma_C = 50)$ plots the probability of having Z pairs of $A-B$. The highest probability of 20% is found for six pairs of type $A-B$. It is also clear that the probability of having 10 or more pairs is extremely small. However, $Z = 6$ is not necessarily the most likely outcome. When a total of 120 tiles is considered, $A = 30$, $B = 40$, and the balance C, the highest probability drops to 15% for 13 pairs, shown in curve $E = P(Z,30,50,40)$. The

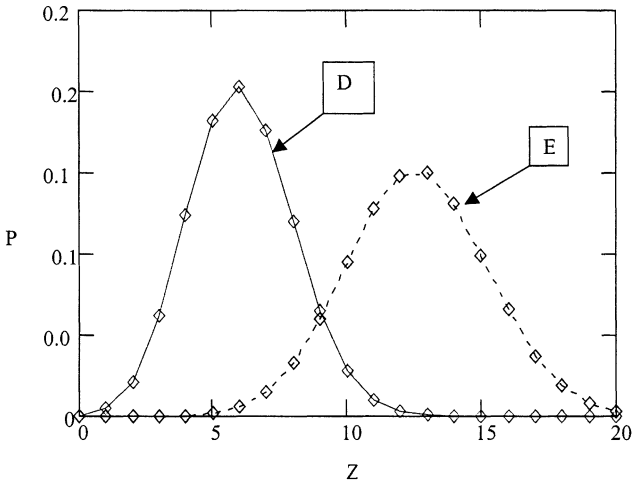

Figure 2. $P(Z, A, B)$ vs. Z.

expectancy value is the most likely Z value that one would find. It is akin to taking an expectation value (by integration) when one has a continuous probability distribution and leads to our main result.

Main Result. Given relative surface areas a and b and the total surface area Γ, the most likely number of $A|B$ contacts is given by the expectancy value

$$\Psi(a, b, \Gamma) = \frac{\sum_{Z=0}^{A} ZP(Z, a, b)}{\Gamma/2} \tag{10}$$

Here $P(Z, a, b)$ is given by Eq. 9. $\Psi(a, b, \Gamma)$ is expressed as a fraction of the total surface area Γ. Equation 7 can be applied to any three-phase problem to determine the expected fraction of all contacts that would be of type $A-B$. It is also applicable in the absence of species C, $a+b=1$, $c=0$, since Eq. 8 is a special case of Eq. 9.

Using this function, one can generate a data set $\Psi(a, b, \Gamma)$, and ideally we would take the limit $\Gamma \to \infty$, but in practice Γ's magnitude would be limited by CPU time. However, as Γ becomes larger, Ψ approaches the limit that is independent of Γ. In Figure 2 $\Psi(a, b)$ is shown for $\Gamma = 1{,}000$. Note that Ψ reaches a maximum when $a=b$, that is, $\sigma_A = \sigma_B$, and it is zero when a and/or b becomes zero. It is convenient to display the expectation values on the triangular domain given by the restrictions $a+b \le 1$ and $b \ge a$ with c implied (since $a+b+c=1$). The factorials have been calculated per definition for small and moderate values and by Stirling's formula for larger values.

Applications of Model

Solid – solid contact area in porous medium and pore sizes

An important application of this theory is found in the determination of solid–solid contact area in the presence of pores. Considerable insight can be garnered from the theory about the pores as well. Either one or two solid species can be considered. The following problem is thus posed: *Given the porosity Φ and particle sizes, determine the $A|B$ contact area and the average pore size*.

The pores are treated as the third species C. If we assign the simple geometric shape of a rhombus to a pore, we need three conditions to determine the principal dimensions of the average pore. However, it is customary to treat pores as cylinders, in which case we only need two conditions. The porosity provides us with one condition and another condition that is readily measured by experiment is the BET-specific surface area, S_{BET}, usually expressed in m^2/g. It is assumed the number of particles of A and B is known, that is, N_A, N_B, but the number of pores, N_C, is not known. Let M_A,M_B denote the mass of A and B, respectively. The pore surface that is in contact with the solid is determined from the BET results. Let us denote this surface as

$$S_{C|A+B} = S_{\mathrm{BET}} \times (M_A + M_B) \tag{11}$$

This is not the total pore area. The total pore area is the sum of pore–solid and pore–pore contacts. The concept of pore–pore contact is a direct consequence of assigning an average shape (cylinder) to the pores. The total pore area is not known, but it can be expressed as

$$S_C = \bar{\omega} S_{\mathrm{BET}} (M_A + M_B) \tag{12}$$

where the factor $\bar{\omega} > 1$ is unknown. Thus, only a fraction of the pore surface is in contact with solids; the balance is pore–pore contact. Pore–solid contact does not distinguish between species A and B.

Thus, A and B can be combined, and we are now dealing with a two-species problem: solids and pores. The algorithm proceeds as follows.

Algorithm 1.

1. Calculate the surface area of species A and B, that is, s_A, s_B.
2. Lump the solid surfaces: $s_s = s_A + s_B$.
3. Calculate $\Gamma = s_s + s_C$
4. Guess $\bar{\omega}$ and calculate s_C from Eq. 12.
5. Determine $\alpha = \min[s_S, s_C]$, $\beta = \max[s_S, s_C]$
6. Calculate $a = \alpha/\Gamma$, $b = \beta/\Gamma$.
7. Calculate $\Psi(a, b, \Gamma)$ from Eq. 7.
8. Calculate the pore–solid contact area $s^*_{\mathrm{CIS}} = \Gamma/2 \times \Psi$
9. Compare $s^*_{C|S} : s_{C|S}$
10. Correct the guess for ω and repeat steps 3–9 until $S^*_{C|S} = S_{C|S}$.

Remark. If only one solid species is present, $s_S = s_A$.

Note. We use the symbol Γ interchangeably to denote the total number of tiles (cf. Eq. 4 or the total surface area (cf. step 3). The reader's attention is drawn to Eq. 5, which converts between tiles and surface area. If α, β is expressed as tiles, Γ must be expressed in tiles to guarantee dimensionless a,b (cf. step 6), and the same holds if α, β is expressed in surfaces, as in step 5.

The converged solution provides the total pore area, s_c. It is trivial to find the pore dimensions if the number of pores is known. To that end we assign to each particle a pore. This is not as restrictive as one may think. It merely states that pores and particles are evenly distributed, and with each particle one can associate a certain pore volume, thence, $N_C = N_{A+B}$. The pore diameter and length are

$$D_P = \frac{4V_{\mathrm{solids}}\Phi}{(1-\Phi)\sigma_C} \tag{13}$$

$$L_P = \frac{\sigma_C}{\pi D_P N_C} \tag{14}$$

Returning to the problem of soslid–solid contact, we first consider the case of one solid species. The solid–solid contact area, $s_{A|A}$, follows directly from the calculation to find the pore–solid contact area. Let A denote the single species. In this case, the solid–pore contact area is $s_{C|A+B} = s_{C|A}$. The total solid surface is either in contact with itself or with pores

$$s_{A|A} = S_A - S_{C|A} \tag{15}$$

When two species are present, the $A|B$ contact area is calculated as follows

Algorithm 2.

1. Determine $\alpha = \min[s_A, s_B]$, $\beta = \max[s_A, s_B]$
2. Calculate $\Gamma = s_A + s_B + s_C$

3. Calculate $a = \alpha/\Gamma$, $b = \beta/\Gamma$
4. Calculate $\Psi(a, b, \Gamma)$ from Eq. 7.
5. Calculate the $A|B$ contact area $s_{A|B} = \Gamma/2 \times \Psi$

The example presented in the fourth section includes details of a pore–solid calculation.

Reaction rate that includes contact area

We develop further arguments using the following generic reaction

$$A(s) + B(s, l, g) \rightarrow C(s, l, g) \tag{16}$$

One reactant is solid at ambient conditions, but the other species may melt during the reaction, or be gaseous. The product could be in any one of the three states. Although our theory is limited to three different competing contact types, it does not mean we cannot accommodate the multiple-product case. We are primarily interested in the $A|B$ contact, because the reaction rate depends on this contact area. The products are just lumped as a single species that competes with the favorable contacts on a statistical basis.

As the chemical reaction proceeds, a and b values change (see definitions 3–5). These changes are due to consumption of particles and other factors such as the fracture and compression and convection of particles. Depending on the mechanism and whether mixing occurs, the expectancy could be calculated once at the onset of the reaction, or continuously through the course of reaction. If one keeps track of these changes, it is possible to map a locus $(a(t), b(t))$ on the $\Psi(a,b)$ surface. The closer the locus remains to the maximum expectancy (region where both a and b are near 0.5), the faster the reaction would be [cf. Richter and Viljoen (2002) for a reaction under mechanical loading that includes compression and fracture]. Low expectancy values could be a result of the small available surface area of either reactant or the interference from the product. For example, the locus may start at or near the apex in Figure 3 (somewhere on the line $a + b = 1 \Rightarrow c = 0$) if there is initially no product, and end at/or close to the point $a = b = 0$ if the reaction goes to completion and the reactant mixture has been near stoichiometric. It is reiterated that applications of the contact theory for reactive mixtures are mechanism-dependent.

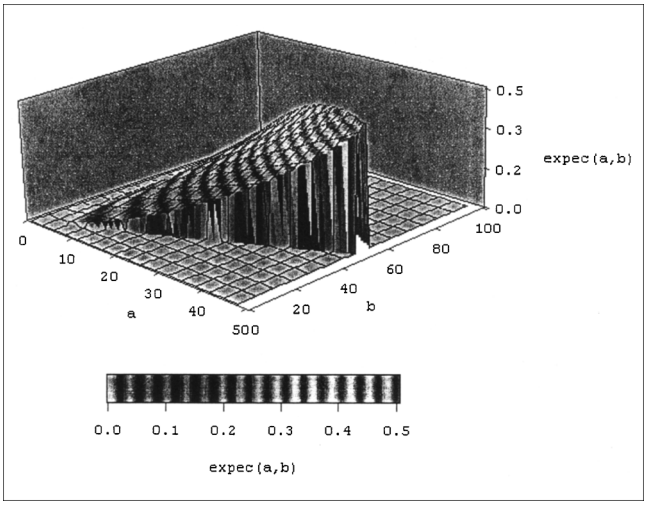

Figure 3. Surface plot of expectancy values.

The primary argument is made that the $A|B$ contact area must be present in a macroscopic kinetic expression. However, before we posit a kinetic expression, a few remarks are in order. The atoms at $A|B$ contacts are in thermal equilibrium. They oscillate in their potential wells in the presence of a thermal bath, and occasionally they occupy the higher end of the Boltzmann distribution and are able to cross the activation energy barrier. This theory was elegantly described by Kramers (1940) and reviewed by Hanggi et al. (1990). Based on statistical arguments, the macroscopic kinetic expression is composed of the number of A and B atoms at the $A|B$ contact area, the fraction of their Boltzmann distributions that has sufficient energy to overcome the activation barrier and a frequency of occurrence of favorable events stemming from the oscillating motions of solids trapped in their potential wells. Thus, we can write

$$r = k_0 C_{AB} d_L^2 \Psi \Gamma e^{-(E/RT)}/2 \tag{17}$$

Note. The usage of d_L implies that Γ is expressed in tiles. If Γ is expressed in surface area, d_L must be omitted in Eq. 17.

The number of A and B atoms at the interface is the concentration of $A|B$ pairs multiplied with the surface-contact area.

The molar surface density of $A|B$ contacts is C_{AB}. It is calculated as follows

$$C_{AB} = \min\left[\frac{1}{d_A^2 N_{Avo}}, \frac{1}{d_B^2 N_{Avo}}\right] \tag{18}$$

The Bohr radii for species A and B are d_A and d_B, respectively, and N_{Avo} is Avogadro's number. Since C_{AB} is known *a priori*, it is a constant. Embedded in $\Psi\Gamma$ reside not only the dependence on particle sizes and shapes, but also the reduction in surface area with consumption, the formation of inhibiting product layers, as well as surface-generating processes like cracking and fracture. Details of the reaction mechanism are also embedded in $\Psi\Gamma$. For example, if the one reactant melts and this is followed by wetting of the solid reactant, the contact area will be affected by this process. Likewise, if a product layer builds up between reactants, $\Psi\Gamma$ is drastically altered and diffusion of one reactant through the product layer will determine the number of $A|B$ pairs. Mathematically speaking, if $\Gamma = \Gamma(t)$ becomes a function of time, the kinetic expression must be complemented with another equation that relates the path dependence of $\Gamma(t)$ as a function of the stress field (in the case of compression, cracking, and fracture), velocity field (convection), temperature (melting and wetting), and concentration gradients (transport through diffusion barriers). However, all these complex factors just influence $\Gamma(t)$, but Eq. 14 remains at the core of the reaction. For details of an application that pertains to a specific mechanism, the reader is referred to Richter and Viljoen (2001).

An important aspect that must be kept in mind is the application of Eq. 14 with the spatial dependence of dependent variables. Then $\Gamma = \Gamma(\bar{x}, t)$, where $\bar{x}$ denotes a position vec-

tor and Γ is expressed in surface area of species per unit volume of the reactor bed. In that case r will carry units of mol/m^3(bed)$\cdot$s. This would find application in chemical waves that involve particulate reactants, typically encountered in combustion synthesis and decoking of catalyst beds.

Examples

Example I: Solid-solid contact in porous medium

Consider a constant volume container, V_{total}, filled with powders A and B to porosity Φ

$$\Phi = 1 - V_{\text{solids}}/V_{\text{total}} \tag{19}$$

The pores are treated as the third species C. The relevant data for this example is listed in Table 1. The average dimensions of particles are known, as is the pore-surface contact area, measured with (for example) the BET method as S_{BET} (m^2/g of solids). Given the molar ratio of A:B, denoted as ϑ, the masses of A and B can be calculated

$$M_A = \frac{V_{\text{total}}(1-\Phi)}{\left(\frac{1}{\rho_A} + \frac{MM_B}{\vartheta MM_A \rho_A}\right)} = 213.44 \text{ g}$$

$$M_B = \frac{M_A \times MM_B}{\vartheta MM_A} = 341.51 \text{ g}$$

The number of particles is

$$N_i = \frac{M_i}{\rho_i \times X_i \times Y_i \times Z_i}$$

that is, $N_A = 6.89 \times 10^{13}$, $N_B = 7.11 \times 10^{13}$. From the ansatz that the total number of pores equals the total number of particles, $N_C = N_A + N_B$. The shape and sizes of the pores are not known. The total surface area of the particles is calculated, using Eqs. 3, 5

$$s_A + s_B = 413.40 \text{ m}^2 + 426.60.0 \text{ m}^2$$

The pore-surface contact area has been measured by BET analysis

$$S_{\text{BET}} \times (M_A + M_B) = 665.94 \text{ m}^2$$

Table 1. Data for Powders

Parameter	Value	Units
V_0	200.0	cm^3
S_{BET}	1.2	m^2/g
Φ	0.3	
X_A	1.0	μm
Y_A	1.0	μm
Z_A	1.0	μm
X_B	1.0	μm
Y_B	1.0	μm
Z_B	1.0	μm
MM_A	0.05	kg/mol
MM_B	0.04	kg/mol
ρ_B	4,800	kg/m^3
ρ_A	3,100.0	kg/m^3
ϑ	1.0	Molar ratio A:B

According to step 4 of Algorithm 1, the total pore area is expressed as $\bar{\omega} S_{\text{BET}}(M_A + M_B)$, where the factor $\bar{\omega} > 1$ is unknown. Thus, only a fraction of the pore surface is in contact with solids; the balance is pore–pore contact. Pore–solid contact does not distinguish between species. Thus, A and B can be combined and we are now dealing with a two-species problem: solids and pores. By definition

$$\Gamma = 413.40 + 426.60 + 665.94\bar{\omega}$$

and it includes the unknown parameter ω. Species A and B are lumped together as solids, and the posed combinatorial problem is just the inverse of previous ones. *We know the solid–pore contact area, but the total pore area is unknown.* It follows from the definitions that

$$a = \min\left(\frac{413.40 + 426.60}{\Gamma}, \frac{665.94\bar{\omega}}{\Gamma}\right)$$

$$b = \max\left(\frac{413.40 + 426.60}{\Gamma}, \frac{665.94\bar{\omega}}{\Gamma}\right)$$

A value is guessed for $\bar{\omega}$; then the expectancy value $\Psi(a,b)$ is calculated. This is the fraction of Γ that constitutes pore-surface contacts; thus

$$\Psi \times \Gamma/2 = S_{\text{BET}} \times (M_A + M_B) = 665.94 \text{ m}^2 \tag{20}$$

Equation 20 is solved iteratively to determine $\bar{\omega} = 3.31$. The final result is $\bar{\omega} = 3.31$. The total pore area is 2,204.26 m^3, but only 665.94 m^2 is in contact with particles; the balance constitutes pore–pore contacts. We do not need the pore dimensions to calculate the contact area between species A and B, but it will be insightful to do it anyway. It follows from Eqs. 13–14 that the diameter and length of a single pore are 0.109 μm and 45.92 μm, respectively.

The total pore area is known, as are the surface areas of the two reactants. This is a regular three-contact problem, and now we can calculate the A/B contact. Let

$$a = \left(\frac{413.40}{\Gamma}\right), \qquad b = \left(\frac{426.60}{\Gamma}\right)$$

then it follows from Eq. 10 that $\Psi = 0.022$. Thus, $\Psi\Gamma/2 = 70.23$ m^2 of the total particle surface area of 840.0 m^2 consists of $A|B$ contact.

Example II: Effect of solid-solid contact on reaction rate

It has been repeatedly pointed out that the details of the mechanism must be known in order to incorporate the correct changes in $\Gamma(t)$. To highlight the competitive role of particle contacts on kinetics, it is better not to tie the example to a specific mechanism; instead the focus remains on Eq. 17

$$r = k_0 C_{AB} d_L^2 \Psi \Gamma e^{-(E/RT_o)}/2$$

Reference Case. A reference rate is calculated for the parameters listed in Table 2. The system is uniformly heated to $T_0 = 1{,}000$ K and the rate is calculated at the onset of the reaction, before consumption of particles and the formation

Table 2.

Parameter	k_0	E	T_0
Value	2×10^6	150,000	1,000
Units	1/s	J/mol	K

of products have altered the statistics of the contact area. All the particles of the reference case are cubes that measure (10 μm$\times$10 μm $\times$10 μm). One mole of A (50 g) and one mole of B (40 g) are mixed. No pores are present. The number of A and B particles and their surface areas are $(N_A;N_B) = (1.61\times10^{+10};\ 8.33\times10^9)$ and $(S_A;\ S_B) = (9.68\ \text{m}^2;\ 5.00\ \text{m}^2)$, respectively. The molar surface density (cf. Eq. 18) is calculated using the Bohr radii listed in Table 1. The expectancy value is $\Psi = 0.224$ and the area of $A|B$ contact is $\Psi\ (s_A + s_B)/2 = 1.65\ \text{m}^2$. Substituting these values into Eq. 17 gives the reference rate. The rates that are scaled by the reference rate are denoted by Ω.

The first effect we want to investigate is size. Both A and B particles remain cubic, but they vary in size between 1 μm and 20 μm. The scaled rate is plotted as a function of the sizes of A and B, and the three-dimensional plot in Figure 4 has the expected monotonic behavior. The rate increases with reduction in particle size. When both species have an average particle size of 20 μm, the rate is only half the reference rate (that is, 10 μm). A linear relation between particle size and rate is observed and the rate increases tenfold when both species have a particle size of 1 μm. However, the relation is not linear when the particle sizes of A and B differ, and interesting conclusions may be drawn. Keep in mind that the expectancy value is maximized when $s_A = s_B$ (cf. apex of Figure 3). At the reference conditions, $s_A > s_B$, and therefore reductions in the particle size of B lead to larger rate increases than reductions in A. Compare the rate of $\Omega = 1.44$ for $(A;B) = (1\ \mu\text{m};\ 10\ \mu\text{m})$ to $\Omega = 2.46$ for $(A;B) = (10\ \mu\text{m};\ 1\ \mu\text{m})$. Not only are different rates observed for the two cases, but diminishing gains will be made through seeking further reductions of the size of A. These asymmetrical results stem from the differences in molar mass and density of the species.

The reaction rate is also affected by particle shape. Conserving volume, surface areas can change by varying shape. This is equivalent to the pure shear deformation of a body. Starting with a 10-μm cube, it is deformed by stretching or compressing along one principal axis of the cube. Thus, two

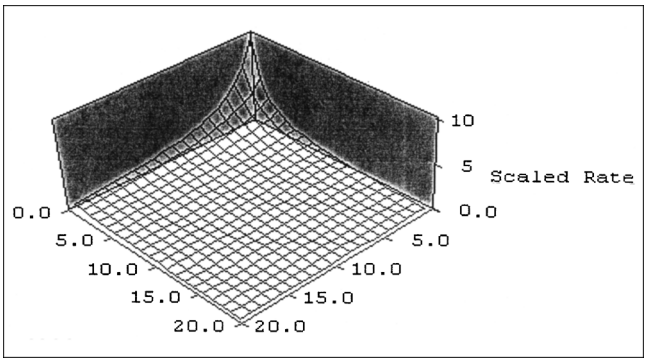

Figure 4. Effect of size of cubic particles on reaction rate.

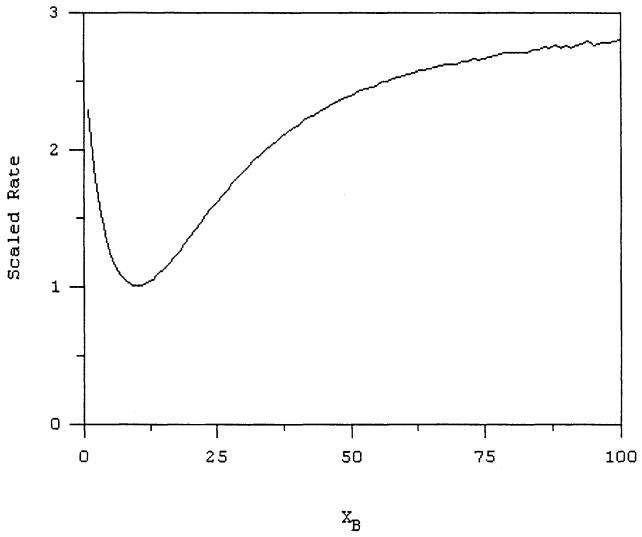

Figure 5. Effect of shape: *B* is transformed from whisker to platelet; *A* is cubic.

sides are kept similar and they are varied between 1 μm and 100 μm. The third dimension is obtained through conservation of volume. When $(X_B,\ Y_B) = (1\ \mu\text{m},\ 1\ \mu\text{m})$, $Z_B = 1{,}000\ \mu\text{m}^3/(X_B \times Y_B) = 1{,}000\ \mu\text{m}$; this is a whisker. At the other extreme lies $(X_B,\ Y_B) = (100\ \mu\text{m},\ 100\ \mu\text{m})$, $Z_B = 0.1\ \mu\text{m}$; this is a platelet. Figure 5 shows the changes in rate when particle B is smoothly transformed from a whisker to a platelet, while particle A remains a $10\times10\times10\ \mu\text{m}^3$ cube. When $X_B = 10$ μm, the reference case is recovered and the scaled rate is $\Omega = 1$. In Figure 5 this is the point at the minimum of the curve. When the B particles are prolate, the surface area increases and the particles become whisker-like. The increase in surface area of B increases the $A|B$ contact area, and the rate increases from $\Omega = 1$ (cube) to $\Omega = 2.28$ (whisker). When X_B increases, the cube is transformed into a platelet and the surface area of these oblate particles increases once again. The reaction rate increases accordingly ($\Omega = 2.79$), but notice that the reaction rate approaches a plateau. When the deformation reaches the point where the surface area of B is larger than the surface area of A, further increases in S_B lead to smaller increases in Ω.

Next the shape of the A particles remains oblate, $(X_A,\ Y_A,\ Z_A) = (100\ \mu\text{m};\ 100\ \mu\text{m};\ 0.1\ \mu\text{m})$, and the B particles are varied. The scaled reaction rates are shown in Figure 6. When whiskers of B are ideally mixed with A, the relative rate is $\Omega = 9.23$. The effective contacts increase significantly compared to the reference case, and the reaction rate increases accordingly. However, the effect is much more dramatic when platelets of both species are mixed. The rate increases to $\Omega = 33.50$. The statistics do not tell us anything about the physical arrangement of this mixture, but a layered structure of sequential platelets of A and B can be contemplated. This would be a microscopic equivalent to the layered foils that Dyer, Munir, and Weihs (1994) have used in their experiments. They have also observed dramatic increases in reaction rates. This analogy cannot be made without qualification, though, since their reactions propagated through the

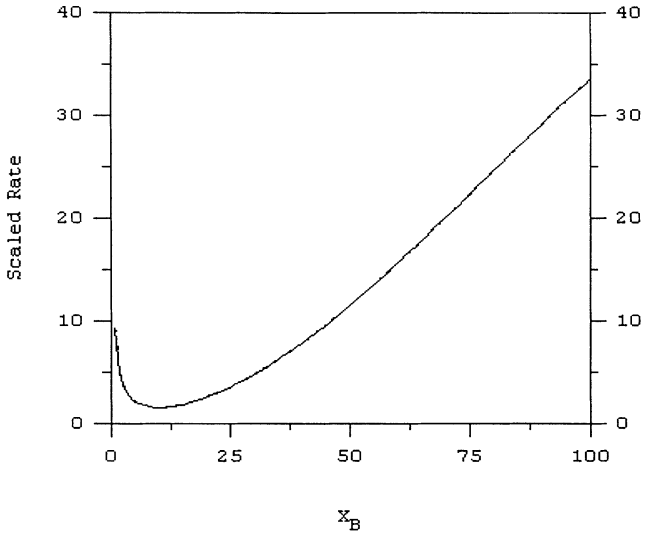

Figure 6. Effect of shape: *B* is transformed from whisker to platelet; *A* is platelet.

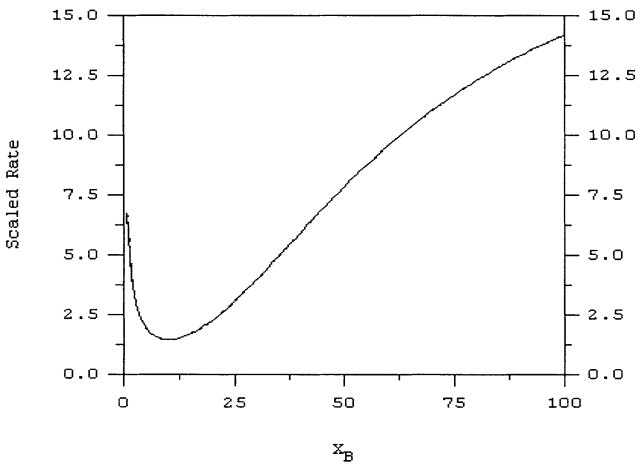

Figure 7. Effect of shape: *B* is transformed from whisker to platelet; *A* is whisker.

system, while we have not addressed the issue of heat transfer.

When the A and B particles are whiskers (1 μm; 1 μm; 1,000 μm), the scaled rate is $\Omega = 6.69$. This case lies (geometrically speaking) diagonally across from the case where both species consists of platelets ($\Omega = 33.50$), and it is evident that platelets are favored over whiskers. In Figure 7 the change in scaled rate is shown for varying B particles between platelets and whiskers, while A particles remain whiskers. The asymmetry is again apparent by comparing the case (A-whiskers, B-platelets), $\Omega = 14.16$ (cf. Figure 7) with the case (A-platelets, B-whiskers), $\Omega = 9.23$ (cf. Figure 6). These examples clearly illustrate that particle shape plays an important role in the observed kinetic rate.

Final Remarks

A combinatorial method has been proposed to determine statistically the expected contact in a three-phase system. The final result is an expression for the expectancy value that depends on the relative surface areas of the different phases. The expression is computationally expensive to solve, but a matrix of data points has been generated that is easily incorporated in any specific application. This matrix and a short code on its implementation are available upon request (contact chrdhjv@engunx.unl.edu).

The applications of this theory extend far beyond solid-state kinetics. For example, the theory finds application in effective medium theories to predict physical and thermal properties of composites or heterogeneous powders. If it is applied in combination with (empirical) models for the coordination number of powders, the average area of a contact can be estimated. It should also contribute toward theoretical models that describe the sintering of green bodies.

The theory has been demonstrated in two examples. The first example addressed the problem of determining the contact area between two different solids, when pores are also present. To the knowledge of the authors, a theoretical solution of this problem has not been proposed before. In order to solve the problem, the porosity and the pore–solid contact area must be known. Both these values can be determined experimentally through routine techniques. Once the total surface area of pores is known, the pore dimensions can be calculated. This calculation is based on two assumptions: (1) the number of pores equals the total number of particles, and (2) the pores have a cylindrical shape. The concept of pore–pore contact is also introduced. This may appear strange at first, but it is analogous to contact between solid particles of the same species.

The second example focused on kinetics. An expression for two-body reactions has been derived, but the complicating details of a specific mechanism were purposefully left out. Two effects have been explored and compared to a reference case. Particle size has the expected effect that smaller particles have a larger surface area and kinetic rates increase. However, the rate is favored by increases in the species with the smaller surface area (with due consideration of stoichiometry, of course). The second effect is particle shape, which it has a rather dramatic effect on the kinetics, as demonstrated by the reaction rates of the equimolar concentrations of the two species, consisting of platelets or whiskers. Reaction rates increase more than thirtyfold when platelets are used, instead of cubes. However, these abridged applications of the theory point to something far more general. The combinatorial method is a powerful tool for bringing particle geometry and size more quantitatively into physical models.

The set of governing equations of a physical model, be it a chemical reaction, sintering, powder compaction, or an effective medium approximation of transport parameters, must be expanded to include the evolution of the particles size and shape. At this stage, the first step demonstrated in Figure 1 becomes important. The abstraction of a complex shape into a simpler geometric shape determines the number of additional evolution equations. If the geometric shape is a cylinder, two equations are needed: the evolution of the average diameter and the evolution of the average length. Likewise one equation is needed for spheres, three for rhombi, and so on. The exact descriptions of these evolution equations depend on the details and specifics of the physical and chemical processes. However, it must be understood that the combina-

torial result stands apart from the mechanism, it becomes an additional variable in a more detailed macroscopic description. It is the evaluation of the expectancy value that necessitates the expansion of the set of governing equations to particle sizes and dimensions. Of course, the treatment of particle sizes as distributions would greatly increase the level of information. In this case the evolution of the distributions will be described by the Fokker–Planck equations, but the computational burden will also increase. Also, $\psi\ (a, b)$ in the kinetics does not merely bring particle sizes and shapes neatly into the kinetic expression, but mechanical and physical processes like fracturing and phase changes become implicitly part of it as well.

The theory stands in need of experimental verification. Exacting experiments must be designed to test the theoretical findings. There are certain practical hurdles, the notion of ideal mixing translates, in experimental terms, into long mixing times. The geometric simplification of complex shapes would be a source of error as well as the approximation of a distribution by an average.

Acknowledgment

The authors thank the National Science Foundation for Financial support through grant CTS0096381.

Notation

a = relative surface area α/Γ
b = relative surface area β/Γ
c = relative surface area σ_C/Γ
C_{AB} = molar surface density $\underset{def}{=} \min[1/(d_A^2 N_{Avo}), 1/(d_B^2 N_{Avo})]$
d_i = Bohr radius
d_L = length scale
D_P = pore diameter $(4V_{\text{solids}}\Phi)/(1-\Phi)\sigma_C]$
E = activation energy
k_0 = frequency factor
L_P = pore length $\sigma_C/(\pi D_P N_C)$
M_i = mass of ith species
MM_i = molar mass of ith species
N_{Avo} = Avogadro's number
N_i = number of particles $M_i/(\rho_i \times X_i \times Y_i \times Z_i)$
$P(Z, \alpha, \beta)$ = probability for Z contacts between two species
$P(Z, \alpha, \beta, \sigma_C)$ = probability for Z contacts in presence of three species
S_{BET} = BET-specific surface area
$s_{i\|j}$ = contact area between species i and j
R = universal gas constant
r = reference rate
s_i = total surface area of ith species
T_0 = reference temperature
V = volume
$\bar{x}$ = position vector
(X_i, Y_i, Z_i) = principal dimensions of ith rhombus
Z = number of pairs of A–B species

Greek letters

$\alpha = \min(\sigma_A, \sigma_B)$
$\beta = \max(\sigma_A, \sigma_B)$
λ = surface roughness
ϑ = molar ratio $A{:}B$
Φ = porosity $(1 - V_{\text{solids}})/V_{\text{total}}$
Γ = total number of tiles or total surface area
σ_i = total number of tiles of a given species
ρ_i = density
Ω = rate scaled by the reference rate
$\Psi(a, b, \Gamma)$ = expectancy value, see Eq. 10

Literature Cited

Anselmi-Tamburini, U., and Z. A. Munir, "The Propagation of a Solid State Combustion Wave in Ni-Al Foils," *J. Appl. Phys.*, **66**, 5035 (1989).

Dyer, T. S., Z. A. Munir, and V. Ruth, "The Combustion Synthesis of Multilayer Ni-Al Systems," *Scr. Met. Mater.*, **30**, 1281 (1994).

Dyer, T. S., and Z. A. Munir, "The Synthesis of Nickel Aluminides from Multilayer Self-Propagating Combustion," *Met. Trans. B*, **26**, 587 (1995).

Frade, J. R., and M. Cable, "Reexamination of the Basic Theoretical Model for the Kinetics of Solid-State Reactions," *J. Amer. Ceram. Soc.*, **75**, 1949 (1992).

Hanggi, P., P. Talkner, and M. Borkovec, "Reaction-Rate Theory: Fifty Years After Kramers," *Rev. Mod. Phys.*, **62**, 251 (1990).

Hwang, S., A. S. Mukasyan, A. S. Rogachev, and A. Varma, "Combustion wave microstructure in gas-solid systems: Experiments and theory," *Combust. Sci. Techol.*, **123**, 165 (1997).

Kieffer, B., C. E. Jones, E. H. Oelkers, and J. Schott, "An Experimental Study of the Reactive Surface Area of the Fontainebleau Sandstone as a Function of Porosity, Permeability, and Fluid Flow Rate," *Geochim. Cosmochim. Acta*, **63**, 3525 (1999).

Kramers, H. A., "Brownian Motion in a Field of Force and the Diffusion Model of Chemical Reactions," *Physica*, **VII**, 284 (1940).

Ma, E., C. V. Thompson, L. A. Clevenger, and K. N. Tu, "Self-Propagating Explosive Reactions in Ni/Al Multilayer Thin Films," *Appl. Phys. Lett.*, **57**, 1262 (1990).

Merzhanov, A. G., "Solid Flames: Discoveries, Concepts and Horizons of Cognition," *Combust. Sci. Flame*, **98**, 307 (1994).

Nan, C-W., X.-P. Li, and R. Birringer, "Inverse Problem for Composites with Imperfect Interface: Determination of Interfacial Thermal Resistance, Thermal Conductivity of Constituents, and Microstructural Parameters," *J. Amer. Ceram. Soc.*, **83**, 848 (2000).

Richter, C., and H. J. Viljoen, "A Combinatorial Approach Towards Solid Phase Reactions," *Thermochim. Acta*.

Smith, J. M., *Chemical Engineering Kinetics*, McGraw-Hill, New York (1981).

Tamhankar, S. S., and L. K. Doraiswamy, "Analysis of Solid-Solid Reactions," *AIChE J.*, **25**, 561 (1979).

Tomasi, R., and Z. A. Munir, "Effect of Particle Size on the Reaction Wave Propagation in the Combustion Synthesis of $Al_2O_3 - ZrO_2 - Nb$ Composites," *J. Amer. Ceram. Soc.*, **82**, 1985 (1999).

Varma, A., A. S. Mukasyan, and S. Hwang, "Dynamics of Self-Propagating Reactions in Heterogeneous Media: Experiments and Model," *Chem. Eng. Sci.*, **56**, 1459 (2001).

Weihs, T. P., "Self-Propagating Reactions in Multilayer Materials," *Handbook of Thin Film Processing Technology*, IOP Publishing, (1997).

Yudson, V. I., M. Schulz, and S. Stepanow, "Dynamics and Roughness of Reaction Fronts in Heterogeneous Solid-Solid Chemical Reactions," *Phys. Rev. E*, **57**, 5053 (1998).

Manuscript received June 20, 2001, and revision received Jan. 22, 2002.